

Analysis of load and adaptability of disc cutters during shield tunneling in soft–hard varied strata

Fengwei YANG^{a,b}, Weilin SU^{a,c*}, Yi YANG^c, Zhiguo CAO^{a,b}

^a Yellow River Engineering Consulting Co., Ltd., Zhengzhou 450003, China

^b Key Laboratory of Water Management and Water Security for Yellow River Basin, Ministry of Water Resources, Zhengzhou 450003, China

^c Key Laboratory of Urban Underground Engineering of Ministry of Education, Beijing Jiaotong University, Beijing 100044, China

*Corresponding author. E-mail: suwelin@126.com

© Higher Education Press 2023

ABSTRACT The disc cutters of shield machines exhibit unsatisfactory adaptability and performance during the soft–hard varied strata tunneling process. To analyze the rotation state, cutting performance, and adaptability of disc cutters during shield tunneling in soft–hard varied strata, the Holmquist Johnson Cook and Federal Highway Administration constitutive models are introduced to numerically simulate the failure process of materials on the excavation face and to calculate the load of disc cutters. Additionally, the parameters of the models are modified based on laboratory disc cutter excavation test results. The results of numerical calculation can reflect the load level and the behavior of the disc cutters during operation. The tangential loads of the disc cutters during the cutting of four typical soft-strata excavation face models are numerically calculated, thus providing reference values for the starting torque of the disc cutters. A greater penetration is suggested for soft-strata tunneling to allow the disc cutters to rotate smoothly and continuously as well as to guarantee a better cutting effect. The disc cutters in the center of the cutterhead should be specified with a lower starting torque to prevent uneven wear, rotation stagnation, cutterhead clogging, and other adverse phenomena.

KEYWORDS shield tunneling, disc cutter load, laboratory excavation test, numerical calculation, soft–hard varied strata

1 Introduction

The shield tunnel machine has been widely used worldwide to construct tunnels, e.g., highway [1], subway [2–4], and water tunnels [5,6]. Compared with the mining tunneling method, the shield tunneling method is more efficient, secure, automated, and eco-friendly [7]. However, it is more sensitive to changes in geological conditions, and the adaptability of the disc cutters and cutterhead may be unsatisfactory when the stratum properties change repeatedly. In particular, the cutterhead typically fails to achieve the expected cutting effect when the disc cutters on it encounter soft strata, such as broken rock, soft rock, and soil layers. Furthermore, eccentric wear often occurs owing to the unsmooth rotation of the

disc cutters, which can significantly reduce the construction efficiency and restrict the application scope of the shield tunneling method [8–13]. The low tunneling efficiency caused by the unsatisfactory adaptability of the disc cutters has become a major obstacle to the efficient tunneling and long-distance tunneling of the shield machine [14]. The cutting load of the disc cutters is a key indicator for evaluating their operating state and cutting performance in shield tunneling projects. However, the disc cutter load changes significantly during the cutting process, particularly in the soft–hard varied stratum cutting situations; furthermore, measuring and sensing the load of every disc cutter during the shield tunneling process are extremely challenging. Therefore, a reliable cutting load calculation method must be devised such that the adaptability of the disc cutters during shield machine tunneling can be investigated.

Numerous investigations have been performed to determine the rock-breaking mechanism and load calculation method of the disc cutter. Evans [15] elaborated the interaction between a disc cutter and a rock. Nishimatsu [16] analyzed the rock breakage and fragment generation that occurred during the operation of a disc cutter. Yang et al. [17] established a three-dimensional rock-breaking model and derived an equation of contacting forces. However, describing the dynamic cutting process of the disc cutters using mechanical models is challenging. Therefore, laboratory tunnel boring machine (TBM) cutting tests were conducted to determine the load state and boring effect of disc cutters operating in various strata. Snowdon et al. [18] investigated the effect of stiffness on the mechanical cutting characteristics of sandstone, granite, and dolerite via a linear rock cutting test and analyzed the load of the disc cutters at various spacings, penetrations, and stiffness levels. Sanio [19] experimentally proved that tensile failure instead of shear failure was the dominant chip-forming mechanism based on a set of sandstone cutting test results. Rostami and Ozdemir [20] established a disc cutter load prediction and optimization model, namely the CSM model, by measuring the stress of the disc cutter ring when linearly cutting granite. Cho et al. [21] presented the results of linear cutting machine tests performed under various cutting conditions to assess the performance of a TBM disc cutter in cutting granitic rock in Korea. Pan et al. [22] conducted several full-scale linear cutting tests to analyze the effect of the confining stress on the cutting force of the disc cutter and discovered that the confining stress, if sufficiently large, can facilitate the rock-breaking process of the disc cutter. To simulate the TBM boring process more realistically, some rotary rock cutting tests, which proved to be different from linear cutting tests in terms of the cutting load and cutting effect [23], were performed using various TBM rotary cutting test devices. Martin et al. [24] reported that rotary rock cutting tests allow TBM performance to be predicted more accurately compared with typically used geotechnical standard tests and full-scale linear cutting tests. Wu et al. [25] investigated the rock fragmentation mechanism and the efficiency of cutter ring insertion for improving TBM excavation efficiency by conducting rotary cutting using an inserted-tooth disc cutter with a diameter of 12 inches. Geng et al. [26–28] proposed an experimental method to investigate the rock-cutting process of TBM gauge cutters using a full-scale rotary cutting machine and discovered that the cutting forces and specific energy of the gauge cutter were lower than those of the normal cutter. The studies above show that performing cutting tests in a laboratory is crucial for determining the rock-breaking mechanism and the load state of disc cutters.

Additionally, numerical simulation methods, including continuous medium methods and the discrete element

method have been attempted to determine the load state of disc cutters operating in various strata. Liu et al. [29] established a finite element model of rock breaking using the R-T^{2d} software to simulate crack formation and propagation during the cutting of single and double disc cutters. Su et al. [30] attempted to identify a method for determining the parameters of the Holmquist Johnson Cook (HJC) constitutive model, based on which the failure process of concrete cut by a shield tool was simulated; additionally, they performed an indoor concrete cutting test to compare and modify the HJC model. Tan et al. [31] used the particle discrete element method to establish a two-dimensional model of a disc cutter cutting rock, investigated the dynamic response of this process, and determined the relationship among rock crack, penetration, and cutting force. Haeri et al. [32,33] estimated the stress intensity factor and the final breakage path in fractured rocks underneath a single disc cutter using a modified higher order semi-infinite displacement discontinuity method. Ren et al. [34] derived a semi-theoretical equation for the inner side force exerting on a cutter ring and analyzed the relationship between cutter ring breakage and inner side force via numerical simulations. Using PFC^{3D}, Wen et al. [35] performed a numerical simulation of a disc cutter breaking rock under different lateral pressure coefficients, cutter spacings, and cutting depths, and then calculated the normal force, rolling force, and damaged particle number. The studies above show that numerical simulation methods are important for investigating the rock-breaking mechanism and calculating the load of disc cutters. However, the methods above are targeted toward hard rock-breaking conditions. The development of shield technology and the expansion of its application scope have enabled disc cutters to be used in soft–hard varied strata; hence, more appropriate constitutive models must be developed to numerically calculate the operating conditions.

In this study, the HJC and Federal Highway Administration (FHWA) constitutive models are used to numerically simulate the failure process of materials on the excavation face in soft–hard varied strata, and the model parameters involved are modified based on laboratory excavation test results of a prototype disc cutter. A load calculation method for disc cutters operating in soft–hard varied strata is devised; subsequently, the cutting performance, rotation state, and adaptability of the disc cutters are analyzed based on the calculation results. The results obtained can serve as a reference for the cutterhead design and operating parameter adoption in soft–hard varied stratum shield tunneling projects.

2 Constitutive models for numerical simulation

Owing to the different mechanisms of the disc cutter in breaking hard rock and cutting soil (which are brittle and

plastic materials, respectively), the appropriate constitutive models should be adopted for numerical simulation. The HJC [36] model was proposed for modeling the crushing failure of concrete materials; it considered the effects of strain rate, damage evolution, confining pressure, crushing, and compaction of the materials. For the soil material cutting process, the excess pore water pressure, strain hardening and softening properties, and strain rate parameters of the material should be considered; hence, the FHWA model, which was proposed to model the shear failure of soil [37], was used to simulate the soil materials on the excavation face.

2.1 Holmquist Johnson Cook constitutive model

The HJC model comprises a strength model, damage evolution model, and state equation.

2.1.1 Strength model

A strength model with normalized equivalent stress can be expressed as

$$\sigma_{\text{eq}}^* = [A(1 - D) + Bp^{*N}](1 + C \ln \dot{\varepsilon}^*), \quad (1)$$

where σ_{eq}^* is the normalized equivalent stress; D is the damage variable, whose value can be determined using the damage model; p^* is the normalized hydrostatic pressure; $\dot{\varepsilon}^*$ is the strain rate; C is the strain rate influence factor, which indicates the enhancement effect of the strain rate on the material strength; A is the normalized viscosity enhancement coefficient; B is the normalized pressure hardening coefficient; and N is the hardening index.

2.1.2 Damage model

The deterioration of brittle materials induced by crack propagation is converted into a damage variable D in the HJC model, and the damage variable D is expressed as

$$D = \sum \frac{\Delta \varepsilon_p + \Delta \mu_p}{\varepsilon_p^f + \mu_p^f}, \quad (2)$$

$$\varepsilon_p^f + \mu_p^f = D_1(p^* + T^*)^{D_2} \geq EF_{\text{MIN}}, \quad (3)$$

where $\Delta \varepsilon_p$ and $\Delta \mu_p$ are the equivalent plastic shear strain increment and the equivalent plastic volumetric strain increment within one integration step in the numerical calculation, respectively; $\varepsilon_p^f + \mu_p^f$ is the plastic strain of the material under the current integration step; T^* is the normalized tensile strength of the material; D_1 and D_2 are the damage constants, which indicate the relationship between plastic strain and normalized hydrostatic pressure; and EF_{MIN} is the minimum plastic strain at the

time of material failure.

2.1.3 State equation

The relationship between volume strain μ and hydrostatic pressure p in the HJC model can be classified into three stages, i.e., elastic, compaction, and compaction deformation. In the elastic stage, a linear relationship exists between μ and p , i.e.,

$$p = K\mu, \quad (p \leq p_c, \mu \leq \mu_c) \quad (4)$$

where K is the bulk modulus, p_c is the limit for the elastic hydrostatic pressure, and μ_c is the limit for the elastic volumetric strain. In the compaction stage, the material is compressed gradually and plastic volume deformation occurs. Therefore, the relationship between μ and p is expressed as

$$p = p_c + K_1(\mu - \mu_c), \quad (p \leq p_1, \mu \leq \mu_1) \quad (5)$$

$$K_1 = (p_1 - p_c)/(\mu_1 - \mu_c), \quad (6)$$

where K_1 is the proportional coefficient of hydrostatic pressure and volumetric strain in the material compaction stage, p_1 is the hydrostatic pressure of compaction, and μ_1 is the corresponding volumetric strain. In the compaction deformation stage, the material is completely crushed without internal forces. Therefore, the relationship between μ and p is expressed as

$$p = K_1\bar{\mu} + K_2\bar{\mu}^2 + K_3\bar{\mu}^3, \quad (7)$$

where K_1 , K_2 , and K_3 are pressure constants. As the material may soften in this stage, the modified volumetric strain $\bar{\mu}$ is introduced, which is expressed as

$$\bar{\mu} = (\mu - \mu_1)/(1 + \mu_1). \quad (8)$$

2.2 Federal Highway Administration constitutive model

The FHWA model comprises an elastic constitutive model, a yield criterion, the excess pore water pressure characteristics, the strain hardening and softening properties, and the strain rate effect.

2.2.1 Elastic constitutive model

The heading face material generates volume strain under the cutting of the disc cutters. The bulk modulus of the material defined in the FHWA model changes with the volume strain and is expressed as

$$K = \frac{K_1}{1 + K_1 D_1 n_{\text{cur}}}, \quad (9)$$

where n_{cur} is the porosity of the material, D_1 is the stiffness control constant of the material before the pore therein collapses, and K_1 is the void-free bulk modulus of the material.

2.2.2 Yield criterion

The improved Mohr–Coulomb yield criterion is adopted in this model, and the yield surface is expressed as

$$f = -p \sin \varphi + \sqrt{J_2 k^2(\theta) + a^2 \sin^2 \varphi} - c \cos \varphi = 0, \quad (10)$$

where p is the hydrostatic pressure, φ is the internal friction angle, c is the cohesion, $k(\theta)$ is the function of the deviatoric plane angle θ , J_2 is the second invariant of the deviator stress, a is the similarity between the modified yield surface and the classical Mohr–Coulomb yield surface.

2.2.3 Strain hardening property

The increment in φ can be expressed as a function of the effective plastic strain of the material to describe the nonlinear strain hardening performance of the material, as follows:

$$\Delta \varphi = H \left(1 - \frac{\varphi - \varphi_i}{N \varphi_{\text{max}}} \right) \Delta \varepsilon_{\text{ep}}, \quad (11)$$

where H is the parameter that determines the nonlinear strain hardening stiffness, N is the fractional value of the peak internal friction angle φ_{max} , φ_i is the initial internal friction angle, and $\Delta \varepsilon_{\text{ep}}$ is the effective plastic strain increment.

2.2.4 Strain softening property

To describe the post-peak strain softening behavior of the material, a damage criterion based on strain energy was established by defining a criterion parameter to measure the damage degree [38–41], as follows:

$$\xi = \frac{1}{K_1} \int \bar{p} d\varepsilon_{\text{pv}}, \quad (12)$$

where \bar{p} is the average effective pressure and ε_{pv} is the plastic volumetric strain.

2.2.5 Strain rate effect

The soil in the excavation face exhibits a high strain rate under the cutting of the disc cutters, which can affect the soil strength. The FHWA model interpolates between the elastic test stress and the inviscid stress [42].

$$\bar{\sigma}_{\text{vp}} = (1 - \zeta) \bar{\sigma} + \zeta \bar{\sigma}_{\text{trial}}, \quad (13)$$

$$\zeta = \frac{1}{\Delta t / \eta + 1}, \quad (14)$$

$$\eta = \left(\frac{\gamma}{\dot{\varepsilon}} \right)^{(V_n - 1) / V_n}, \quad (15)$$

where $\bar{\sigma}_{\text{trial}}$ is the elastic test stress after material damage; $\bar{\sigma}$ is the cohesionless stress; and V_n and γ are the strain rate strength enhancement effect parameters, which are a set of constants that indicate the material strength enhancement effect of the strain rate.

2.2.6 Excess pore water pressure

Based on the effective stress principle of soil, the internal stress of the material exhibits the following relationship:

$$p' = p - u, \quad (16)$$

where p' and u are the effective stress and pore water pressure of the material, respectively.

2.3 Parameter assignments of constitutive model keyword file

The material parameters of the finite element model were assigned by defining the keyword files for the HJC and FHWA models, in which the density ρ , shear modulus G , tensile strength T , and uniaxial compressive strength (UCS) f_c are measured based on a test standard [43]. In addition, the strength parameters (A , B , and N), state equation parameters (K_1 , K_2 , and K_3), rate effect parameter (C), and damage parameters (D_1 , D_2 , and F_{MIN}) are assigned using methods described in Ref. [30].

For the FHWA model, the elastic parameters (K and G) of the material can be measured via triaxial compression tests. Meanwhile, the strength parameters (c and φ) are measured via direct shear tests or triaxial tests. The moisture of the soil can be measured using the drying method. Additionally, the yield surface similarity A is associated with the cohesion and internal friction angle of the material and can be expressed as follows:

$$a = \frac{c}{20} \cot \varphi. \quad (17)$$

Meanwhile, the failure of the soil under the cutting of the disc cutters is a typical problem involving high strain rates. Therefore, the strain rate parameters (V_n and γ) in the numerical calculation should be calibrated based on the excavation test results, and the other FHWA model parameters can be set based on previous studies [37]. The material parameters of the excavation face model were determined by geotechnically testing the C30 concrete

and soil used in the excavation test, which will be described later. The preliminary values of the HJC and the FHWA constitutive model parameters are shown in Table 1.

Based on the model parameters in Table 1, for the materials that exhibit a clear plastic deformation stage, the FHWA model considers the yield criterion as well as the strain hardening and softening properties. Meanwhile, the HJC model primarily considers the damage and crushing process, thus rendering it more suitable for the evaluation of brittle materials.

3 Excavation test in soft–hard varied strata

A prototype disc cutter excavation test in soft–hard varied strata was performed, based on which the numerical calculation results were verified and the parameters adopted were modified.

3.1 Laboratory excavation test using prototype disc cutters

The test was performed on the excavation test platform (Fig. 1) in the State Key Laboratory of Shield and Boring Technology in Zhengzhou, China. This test platform was used to conduct a laboratory full-scale cutting test using a disc cutter in this study. In total, four disc cutters (18 inches in diameter) were installed on the cutterhead of the test platform and successively arranged from the inside to the outside of the cutterhead, from No. 1 to No. 4. The measurement system comprised a load measurement system, speed measurement system, torque measurement system, and displacement measurement system, where the load was measured by force sensors, the displacement by guyed displacement sensors, and the speed and torque by torque–speed sensors. The control system was formed by the cutterhead advancement control system and the disc cutter spacing control system.

To simulate the operating condition of the disc cutter during shield tunneling in soft–hard varied strata in this laboratory test, we established an excavation face model using four different types of materials: C30 concrete, C15 concrete, M2.5 cement mortar, and soil (numbered 1, 2, 3, and 4, respectively, in Fig. 2).

The amount required of the materials was calculated based on the “Specification for Mix Proportion Design of Ordinary Concrete” (JGJ 55–2011) [44] and the “Specification for Mix Proportion Design of Masonry Mortar” (JGJ/T 98–2010) [45]. The ratio and dosage of the materials are shown in Table 2.

Three concrete or cement mortar specimens (100 mm × 100 mm × 100 mm) for each type of material listed in Table 2 were prepared, and their UCS was tested using a WAW-1000 universal testing machine. The curing

Table 1 Parameter assignments of the HJC and FHWA constitutive models

model type	parameter type	parameter assignment	value
HJC model	basic parameters	ρ (kg/m ³)	2110
		G (MPa)	8.75×10^3
		T (MPa)	1.62
		f_c (MPa)	24.45
	strength parameters	A	0.272
		B	1.50
		N	0.87
		SF_{MAX}	20
		state equation parameters	p_1 (MPa)
	μ_1		0.16
	p_c (MPa)		8.15
	μ_c		6.99×10^{-4}
	K_1 (GPa)		9.23
	K_2 (GPa)		141.24
	strain rate effect parameters	K_3 (GPa)	136.50
C		0.012	
ESP_0		1.0	
damage parameters		D_1	0.04
	D_2	1.0	
	EF_{MIN}	0.01	
FHWA model	basic parameters	ρ (kg/m ³)	1408.7
		ρ_w (kg/m ³)	1.00
		G_s	1.80
	elastic parameters	K (MPa)	11.03
		G (MPa)	5.09
	yield parameters	D_1	0
		c (MPa)	2.21×10^{-2}
		φ (°)	24.4
		a	2.37×10^{-3}
	excess pore water pressure parameters	ω	0.033
		D_2	0
	strain hardening and softening parameters	AN	0
		D_{int}	5.0×10^{-5}
		φ_{max} (°)	40
	strain rate effect parameters	V_n	0
γ		0	

conditions of these specimens were the same as those of the excavation face model (covering and watering for 28 d at room temperature). The average UCS of each type of material is listed in Table 3. Additionally, six cylindrical saturated soil samples were formed; subsequently, their shear strength parameters (c and φ) and those of the

soil were tested via conventional triaxial (consolidated drainage) tests. In addition, the moisture and density of the soil were tested based on the Standard for Geotechnical Test Methods (GB/T 50123-2019) [46].

The excavation face model was bored after the curing process when the load of the disc cutters was monitored and recorded using the sensors and computer. The operating parameter of a shield machine should be controlled and adjusted accordingly based on the properties of strata involved in tunneling projects. Generally, the advancing rate (v) is set to 0.5–20 mm/min

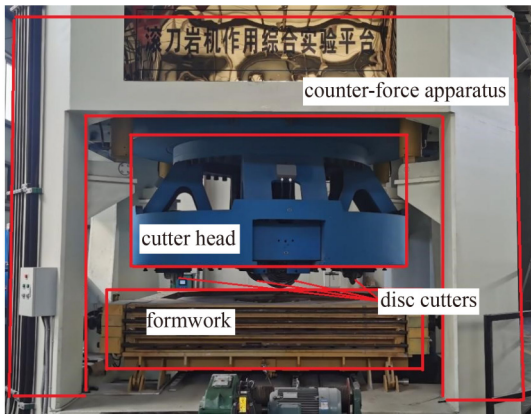


Fig. 1 Excavation test platform.



Fig. 2 Excavation face model in soft-hard varied strata.

Table 2 Material ratio and consumption per cubic meter

material type	cement grade	water (kg)	sand (kg)	coarse aggregate (kg)	water-cement ratio	sand ratio
C30 concrete	425	223	618	1023	0.47	0.37
C15 concrete	325	184	655	1271	0.61	0.34
M2.5 mortar	325	310	1450	–	–	–

Table 3 Uniaxial compressive strength of different materials

material type	test strength (MPa)
C30 concrete	27.7
C15 concrete	12.1
M2.5 mortar	3.2

and 0 and the rotation speed of the cutterhead (ω) is set to 0.5–4 r/min. Meanwhile, the spacing between two adjacent disc cutters (S) is typically 80–120 mm for a cutterhead used for boring in soft-hard varied strata. Therefore, to simulate the actual situation, the cutter spacing was set to 100 mm, and the rotation speed and advancing rate of the cutterhead were set to 1 r/min and 3 mm/min, respectively. To maintain the accuracy of the test results, debris from the excavation face model should be removed timely during the test. The excavation face model of soft-hard varied strata after being bored is shown in Fig. 2.

After being bored, the C30 concrete, C15 concrete, and M2.5 cement mortar were crushed into fragments, and the uniformity and fractal characteristics of the debris generated by each material differed from each other. The soil exhibiting plasticity was extruded between two cutting paths and was not crushed. This type of plastic material will accumulate on the excavation face and adhere to the cutterhead if not removed timely. In shield tunneling projects, the accumulation of plastic materials on the excavation face may cause cutterhead clogging, which can further deteriorate the boring ability of the shield machine.

3.2 Comparison between numerical calculation and tunneling test results

3.2.1 Numerical calculation of excavation face bored by disc cutters

A finite element model of a one-eighth circumference excavation face being bored by two adjacent disc cutters (the diameter of the cutter rings = 18 inches) was established, as shown in Fig. 3; the disc cutter spacing, rotation speed, and advancing rate of the model were set the same as those used in the laboratory excavation test ($S = 100$ mm; $\omega = 1$ r/min; $v = 3$ mm/min). In the numerical calculation, the impact between the disc cutter

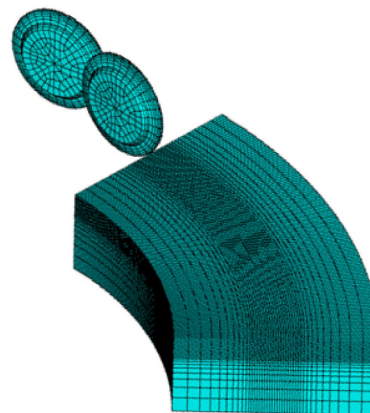


Fig. 3 Finite element model of the excavation face and disc cutters.

ring and excavation face was primarily considered. To consider both the calculation efficiency and accuracy, the material of the disc cutter rings was set to elastic–plastic, and the other sections of the disc cutters were modeled as rigid bodies.

One-eighth of the excavation face was modeled in this study, and the HJC and FHWA model parameters were assigned by defining the keyword files based on Table 1 to simulate C30 concrete and soil, respectively. Full replacement constraints were applied to the bottom of the excavation face model, whereas normal constraints were applied to its side. Subsequently, the finite element model was imported to LS-DYNA, which is a geometrically nonlinear (large displacement, rotation, and strain) calculation program, where the rotation and revolution of the disc cutters were defined to simulate the cutting process. After the excavation face cutting by the disc cutter was simulated, the strain of the excavation face after being bored was obtained, as shown in Fig. 4.

The maximum residual strains of the excavation face models based on soil and C30 concrete were 0.67 and 0.28, respectively (see Fig. 4). The residual strain distribution reveals the difference between the brittle and plastic materials, i.e., failure occurs when the strain of the concrete material is small and the soil indicates a larger extreme strain. Additionally, by comparing the residual strain distributions from the numerical simulation, the disc cutters based on the HJC model shows a larger destruction scope.

3.2.2 Parameter modification of HJC and FHWA models

For the boring of C30 concrete, the tangential cutter load, whose direction is parallel to the excavation face, was acquired from the laboratory excavation test and numerical simulation, and the results are shown in Fig. 5.

Before the parameter was modified, the numerical simulation results based on the HJC model fitted the laboratory test results relatively well (see Fig. 5).

However, the mean value and volatility of the former were all lower than those of the latter. Because the strain rate parameter C and damage parameter D_1 were assigned empirically, several possible values were assigned to the two parameters; subsequently, a set of values ($D_1 = 0.02$; $C = 0.06$) was selected when the numerical simulation results were similar to the test data. The parameter modifying process is shown in Fig. 6. The tangential load of the disc cutter load obtained via numerical simulation based on the HJC model is shown in Fig. 5.

Similarly, the uncertain parameters in the FHWA model were modified using the same method ($V_n = 1.1$; $\gamma = 0.1$), and the simulation results for the tangential load of the disc cutter before and after parameter modification are shown in Fig. 7.

4 Analysis of numerical simulation results and adaptability of disc cutters

After performing parameter modification based on a comparison with the laboratory test results, the cutting process of the disc cutters was numerically simulated. The load of the disc cutters when cutting different types of strata under different operating conditions was calculated, based on which the adaptability of disc cutters during shield tunneling in soft–hard varied strata was analyzed.

4.1 Analysis of disc cutter cutting performance in soft–hard varied strata

The disc cutter is custom designed to break hard rocks and comprises a narrow blade to provide sufficient rock-breaking pressure. If soil layers or soft rock exist on the excavation face, owing to their high plasticity and large residual deformation, the materials above will not detach easily after being cut by the disc cutter. Subsequently, the residual soil or soft rock may accumulate on the cutter shaft and compact gradually, resulting in disc cutter

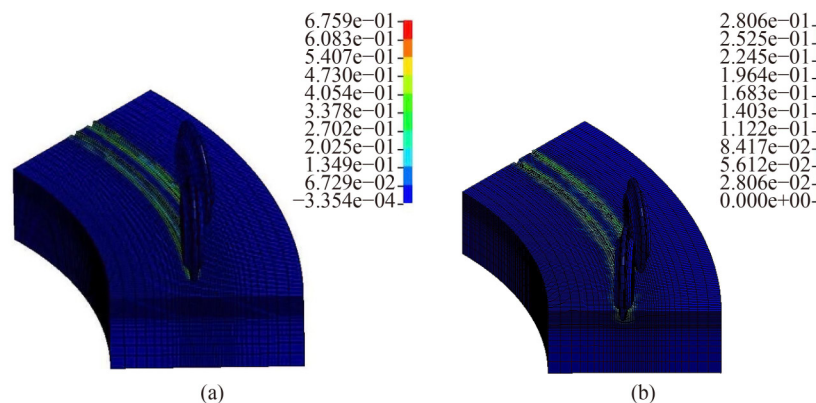


Fig. 4 Residual strain distribution obtained from numerical simulations: (a) soil cutting numerical simulation based on the FHWA model; (b) concrete cutting numerical simulation based on the HJC model.

rotation stagnation and in some cases, cutterhead clogging. Therefore, when performing shield tunneling in soft–hard varied strata, the cutting performance of the disc cutter in soft strata must be prioritized. The simulation result obtained in this study shows that the cutting depth (H) of the disc cutter rings significantly affects soil cutting, as shown in Fig. 8.

Based on Fig. 8, significant strain concentrations occurred in the element positioned near the two cutting paths in the simulation. A comparison of the number of remaining elements shows that as the cutting depth decreased, the number of model elements between the cutting traces that did not vanish during cutting as well as the equivalent strain of these elements increased. Therefore, when soil or soft rock layers are present on the excavation face, owing to the non-adjustable disc cutter spacing, an appropriately large cutting depth should be adopted to ensure a better stratum-cutting effect.

4.2 Disc cutter load and its influencing factors

Based on the numerical calculation results obtained using the HJC model, the curves of the tangential load of the disc cutter over time under different cutting depths and cutting speeds (determined by the rotation speed of the cutterhead) were constructed, are shown in Figs. 9 and 10, respectively. To control a single variable on the disc cutter load, the rotation speed was fixed to 1 r/min to investigate the effect of the cutting depth, whereas the cutting depth was fixed to 3 mm to investigate the effect of the cutting speed.

Based on Figs. 9 and 10, when boring the rock stratum, the tangential load of the disc cutter increased with the cutting depth, and the load fluctuation intensified. Meanwhile, as the cutting speed increased, the load of the disc cutter increased and its fluctuation amplitude

decreased. Based on Fig. 8, the disc cutter required different durations to cut the same excavation face model at different cutting speeds.

Based on the numerical calculation results obtained using the FHWA model, the curves of the tangential load of the disc cutter over time under different cutting depths and cutting speeds were constructed, as shown in Figs. 11 and 12, respectively.

Based on Figs. 11 and 12, when cutting the soil stratum, the tangential load of the disc cutter also increases with the increase of the cutting depth and the cutting speed. However, compared with the cutting rock stratum situation, the cutting depth of the cutter ring in the soft stratum has a greater impact on the load of the disc cutter. It is found that the load of the disc cutter in the soft stratum is only 1/80–1/100 of that in the hard rock stratum. At this time, although the impact and damage to the disc cutters caused by the cutting load are small, the tangential load cannot provide the starting torque, which causes more rotation stagnation of the disc cutters.

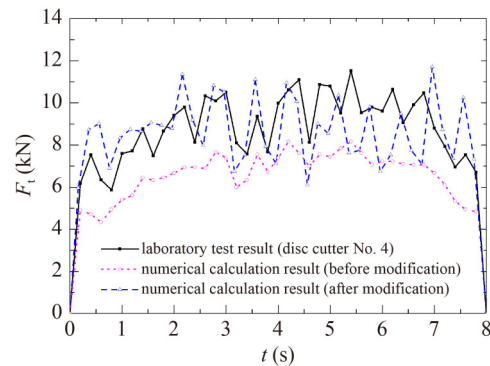


Fig. 5 Comparison and correction of numerical calculation results based on the HJC model.

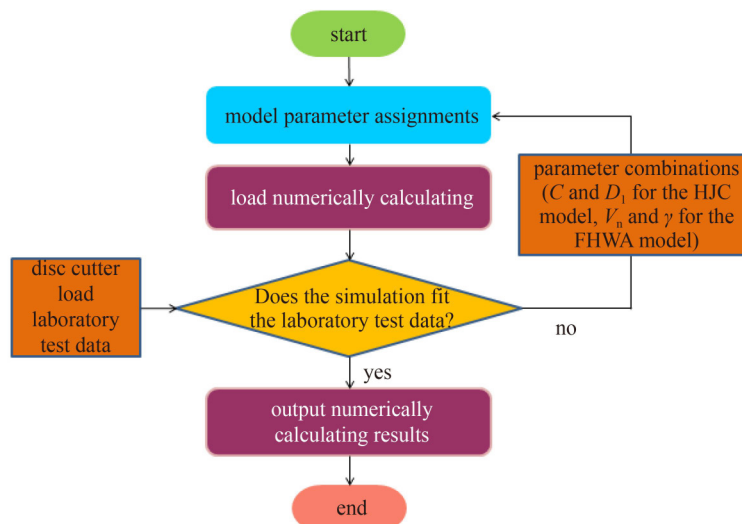


Fig. 6 Flowchart of the constitutive model parameter modification.

4.3 Starting conditions of disc cutter in different stratum types

To improve the bearing stiffness and reduce the damage by vibration and impact load to the bearing, disc cutters are generally pretensioned to reduce the clearance between the ring and hub of the cutter rings. For a disc cutter, a certain torque is required to induce its rotation, which is known as the starting rotation. The starting torque of the 18-inch disc cutters used in the laboratory test was measured using an electronic torque wrench (see Fig. 13).

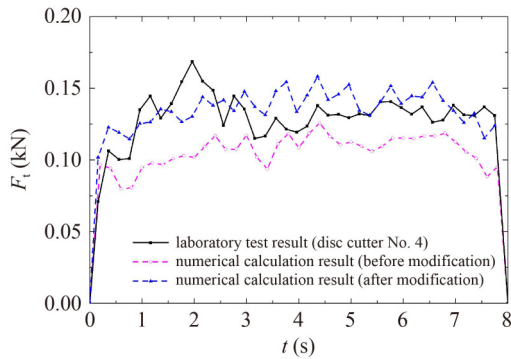


Fig. 7 Comparison and correction of numerical calculation results based on the FHWA model.

The starting torques of the No. 1 to No. 4 disc cutters used in this test were measured to be 39.6, 38.2, 41.1, and 42.6 N·m, respectively. After conversion, the minimum tangential load required to start the rotation of all the disc cutters in the test was 0.186 kN. In fact, the starting torque of the disc cutters is typically set empirically during shield tunneling, i.e., it is a fixed value for the same cutting ring size under any stratum. For example, the starting torque of all 18-inch disc cutters is set to 50 N·m. However, based on the findings above, disc cutters exhibit different tangential loads under different strata and tunneling parameters, and uneven wear occurs when the tangential load fails to start the rotation of a disc cutter. Furthermore, because the cutter ring profile is no longer a circle, restarting the disc cutter rotation become more difficult even if the FT is sufficiently large. Consequently, the disc cutters will fail to cut the excavation face as intended. If not addressed timely, the uneven wear and rotation stoppage can result in crushing failure on the excavation face and cutterhead clogging, thus causing the cutting ability of the disc cutters to vanish almost completely. Therefore, the tangential load of the disc cutters must be calculated when performing shield tunneling in strata of different strengths; subsequently, the adaptability must be evaluated and the appropriate starting torque for disc cutters in soft strata

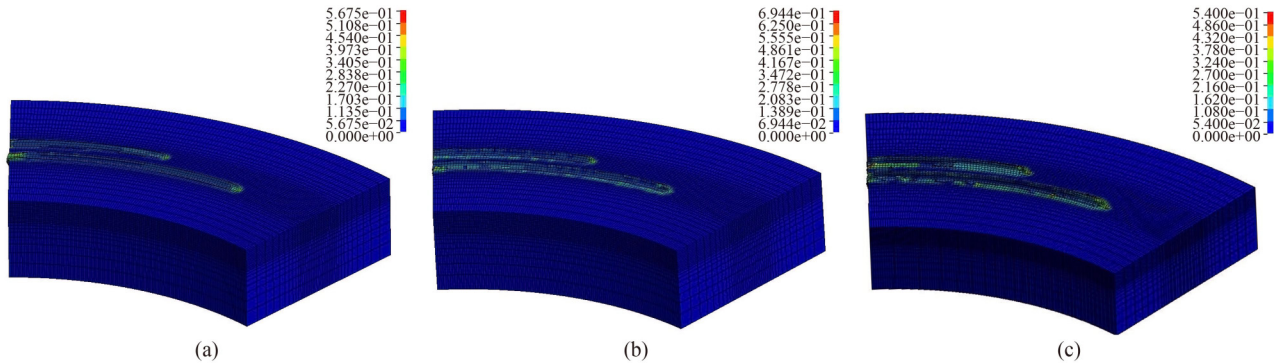


Fig. 8 Equivalent stress dynamic distribution in soft-stratum cutting: (a) $H = 1.0$ mm; (b) $H = 3.0$ mm; (c) $H = 6.0$ mm.

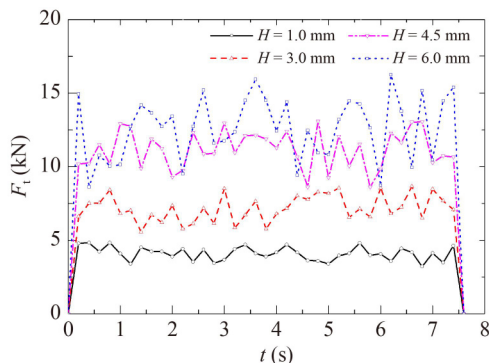


Fig. 9 Disc cutter load vs. time at different cutting depths (based on the HJC model).

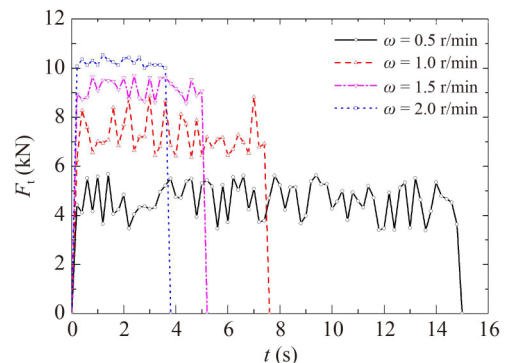


Fig. 10 Disc cutter load vs. time at different cutterhead rotation speeds (based on the HJC model).

must be determined.

To provide reference values for the tangential load of disc cutters under different strata and tunneling

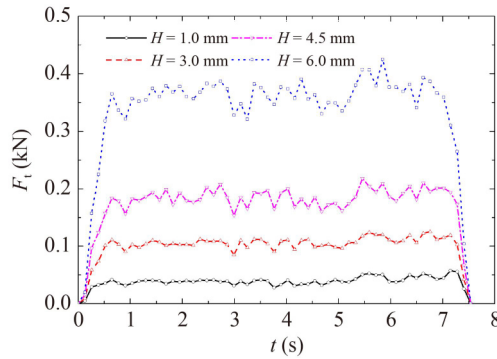


Fig. 11 Disc cutter load vs. time at different cutting depths (based on the FHWA model).

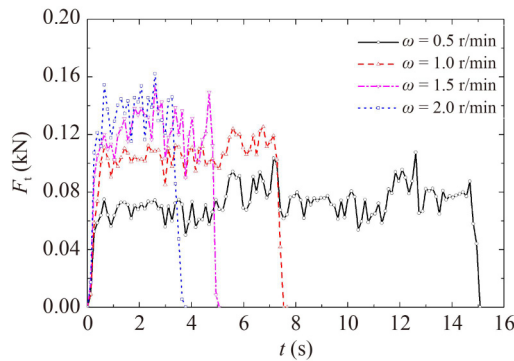


Fig. 12 Disc cutter load vs. time at different cutterhead rotation speeds (based on the FHWA model).



Fig. 13 Starting torque measurement of the disc cutter.

parameters, the boring process was numerically simulated; additionally, four types of typical soil and soft rock materials involved in shield tunneling were simulated based on the FHWA model. The parameters of the FHWA model are listed in Table 4.

The tangential loads of the disc cutter when cutting the four types of materials listed in Table 4 were calculated, and the mean and variance of the calculation results are shown in Figs. 14 and 15.

Based on Figs. 14 and 15, under the tunneling conditions of this study, the maximum tangential loads of the disc cutter when cutting strongly weathered sandy conglomerate, sandy gravel hard soil, hard soil, and ordinary soil were 0.55, 1.65, 5.04, and 6.34 kN, respectively. As the cutting depth increased, the tangential load of the disc cutter increased linearly in the strongly weathered conglomerate and sandy gravel hard soil, whereas the increase intensified gradually in the hard soil and ordinary soil. In other words, the stronger the plasticity of the material being cut, the greater is the effect of the cutting depth. This is because, for the materials with high plasticity, more model elements remained in contact with the cutter ring after cutting was performed, which is consistent with the actual situation. For the strongly weathered conglomerate and sandy gravel solid soil, the volatility of the tangential load of the disc cutter increased with the cutting depth. Meanwhile, when the penetration increased, the energy accumulation and release processes intensified.

In addition, because the FHWA model includes the strain rate parameters that affect the dynamic strength of the materials, the tangential load of the disc cutter increased slightly with the rotation speed of the cutterhead, and the volatility of the load decreased gradually. Therefore, disc cutters with different installation radii on the cutterhead should be set with different starting torques. In particular, the disc cutters with a low cutting linear speed in the center of the cutterhead should be set with a smaller starting torque to prevent uneven wear, rotation stagnation, cutterhead clogging, and other adverse phenomena. The numerical calculation results can serve as a reference for the cutterhead design and operating parameter adoption in soft–hard varied stratum shield tunneling projects.

Table 4 Parameter values of the FHWA constitutive model for different materials

soil type	FHWA model parameter values									
	ρ (kg/m ³)	K (MPa)	G (MPa)	c (kPa)	φ (°)	φ_{\max} (°)	AN	D_{int}	V_n	γ
ordinary soil	1408	9.8	2.3	17.41	25.2	40	0	5.0×10^{-5}	1.1	0.10
hard soil	1514	51.8	22.1	13.35	27.6	42	0	5.0×10^{-5}	1.2	0.10
sandy gravel hard soil	1920	125.4	51.0	25.90	30.7	45	0	5.0×10^{-5}	1.2	0.10
strongly weathered sandy conglomerate	2050	208.5	112.6	42.00	34.7	45	0	5.0×10^{-5}	1.2	0.15

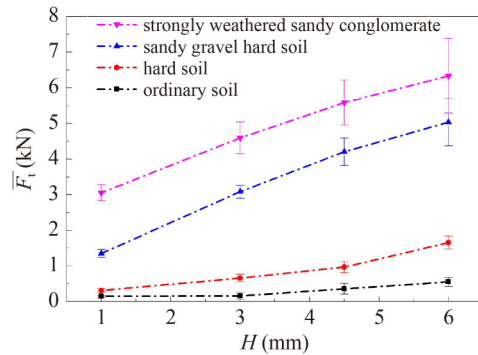


Fig. 14 Mean and variance of disc cutter load vs. cutting depth.

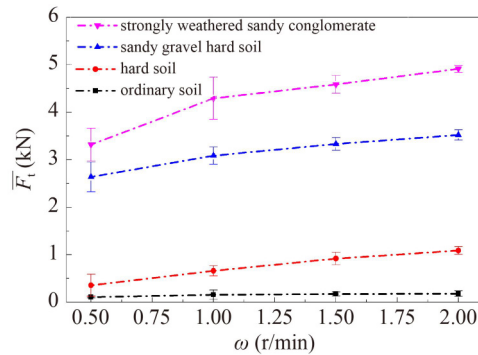


Fig. 15 Mean and variance of disc cutter load vs. rotation speed of cutterhead.

5 Conclusions

In this study, the HJC and FHWA models were used to numerically simulate the failure process of materials on the excavation face in soft–hard varied strata. Subsequently, the load of the disc cutters was calculated and the uncertain model parameters in these two dynamic constitutive models were modified based on laboratory excavation test data. Next, the cutting performance, rotation state, and adaptability of the disc cutters were analyzed based on the calculation results. The main conclusions obtained are as follows.

1) The load of the disc cutters and its variety during shield tunneling in soft–hard varied strata can be calculated via numerical simulation using the FHWA and HJC constitutive models. Meanwhile, the uncertain parameters (the strain rate parameter C and the damage parameter D_1 for the HJC model; the strain rate parameters V_n and γ for the FHWA model) were modified via laboratory excavation tests.

2) Based on the modified FHWA model, the tangential loads of the disc cutters in four typical soft–strata excavation face models were calculated, which serve as reference values for the starting torque of disc cutters in soft–hard varied strata required in shield tunneling projects.

3) The calculation results showed that an appropriately larger penetration cannot only increase the tangential load of the disc cutter and ensure the smoothness of its rotation, but also facilitate larger element equivalent strains between cutting tracks and guarantee a better stratum-cutting effect.

4) The tangential load of the disc cutter increased with the cutting speed, as shown by the numerical calculation results. The disc cutters with a low cutting linear speed in the center of the cutterhead should be set with a smaller starting torque to prevent uneven wear, rotation stagnation, cutterhead clogging, and other adverse phenomena.

Acknowledgements The authors gratefully acknowledge the financial support provided by the National Key R&D Program of China (No. 2020YFF0426370) and the National Natural Science Foundation of China (Grant No. 51978040).

References

- Liao S M, Peng F L, Shen S L. Analysis of shearing effect on tunnel induced by load transfer along longitudinal direction. *Tunnelling and Underground Space Technology*, 2008, 23(4): 421–430
- Shen S L, Xu Y S. Numerical evaluation of land subsidence induced by groundwater pumping in Shanghai. *Canadian Geotechnical Journal*, 2011, 48(9): 1378–1392
- Jin D L, Yuan D J, Li X G, Zheng H T. An in-tunnel grouting protection method for excavating twin tunnels beneath an existing tunnel. *Tunnelling and Underground Space Technology*, 2018, 71: 27–35
- Jin D L, Yuan D J, Li X G, Zheng H T. Analysis of the settlement of an existing tunnel induced by shield tunnelling underneath. *Tunnelling and Underground Space Technology*, 2018, 81: 209–220
- Yagiz S, Karahan H. Application of various optimization techniques and comparison of their performances for predicting TBM penetration rate in rock mass. *International Journal of Rock Mechanics and Mining Sciences*, 2015, 80: 308–315
- Min F L, Du J R, Zhang N, Chen X G, Lv H J, Liu L C, Yu C J. Experimental study on property change of slurry and filter cake of slurry shield under seawater intrusion. *Tunnelling and Underground Space Technology*, 2019, 88: 290–299
- Zhu W, Qian Y J, Min F L, Wang L, Wang C, Xu C, Hu J N. The current status and some problems of slurry shield in China. *Tunnel Construction*, 2019, 39(5): 724–735 (in Chinese)
- Sun W, Shi M L, Zhang C Z, Zhao J, Song X. Dynamic load prediction of tunnel boring machine (TBM) based on heterogeneous *in-situ* data. *Automation in Construction*, 2018, 92(8): 23–34
- Yang Y, Li X G. Review on the issue of clogging occurred in shield tunnelling. *Chinese Journal of Underground Space and Engineering*, 2020, 16(S2): 1030–1038 (in Chinese)
- Zhang N C. Analysis of wear shape of disc-cutter edge of

- TBM/shield and optimization measures. *Tunnel Construction*, 2021, 41(4): 657–665 (in Chinese)
11. Zhu W B, Ju S J. *Technology for Shield Tunnelling in Mixed Face Ground Condition*. Beijing: Science and Technology of China Press, 2006 (in Chinese)
 12. Ren D J, Shen S L, Arulrajah A, Cheng W C. Prediction model of TBM disc cutter wear during tunnelling in heterogeneous ground. *Rock Mechanics and Rock Engineering*, 2018, 51(11): 3599–3611
 13. Ren D J, Shen S L, Zhou A, Chai J C. Prediction of lateral continuous wear of cutter ring in soft ground with quartz sand. *Computers and Geotechnics*, 2018, 103: 86–92
 14. Li X G, Li X C, Yuan D J. Application of an interval wear analysis method to cutting tools used in tunnelling shields in soft ground. *Wear*, 2017, 392–393: 21–28
 15. Evans I. The force required to cut coal with blunt wedges. *International Journal of Rock Mechanics and Mining Sciences & Geomechanics Abstracts*, 1965, 2(1): 1–12
 16. Nishimatsu Y. The mechanics of rock cutting. *International Journal of Rock Mechanics and Mining Sciences & Geomechanics Abstracts*, 1972, 9(2): 261–270
 17. Yang H Q, Wang H, Zhou X P. Analysis on the damage behavior of mixed ground during TBM cutting process. *Tunnelling and Underground Space Technology*, 2016, 57(Aug): 55–65
 18. Snowdon R A, Ryley M D, Temporal J, Crabb G I. The effect of hydraulic stiffness on tunnel boring machine performance. *International Journal of Rock Mechanics and Mining Sciences & Geomechanics Abstracts*, 1983, 20(5): 203–214
 19. Sanio H P. Prediction of the performance of disc cutters in anisotropic rock. *International Journal of Rock Mechanics and Mining Sciences & Geomechanics Abstracts*, 1985, 22(3): 153–161
 20. Rostami J, Ozdemir L. New model for performance production of hard rock TBMs. In: *Proceedings of the 1993 Rapid Excavation and Tunnelling Conference*. Boston: Energy Data Base, 1993, 793–809
 21. Cho J W, Jeon S, Jeong H Y, Chang S H. Evaluation of cutting efficiency during TBM disc cutter excavation within a Korean granitic rock using linear-cutting-machine testing and photogrammetric measurement. *Tunnelling and Underground Space Technology*, 2013, 35: 37–54
 22. Pan Y C, Liu Q S, Liu J P, Peng X X, Kong X X. Full-scale linear cutting tests in Chongqing sandstone to study the influence of confining stress on rock cutting forces by TBM disc cutter. *Rock Mechanics and Rock Engineering*, 2018, 51(6): 1697–1713
 23. Gong Q M, Miao C T, Ma H S, Zhao X B. Effect of joint spacing on rock breaking under disc cutter by linear cutting experiments. *China Civil Engineering Journal*, 2015, 48(6): 97–105 (in Chinese)
 24. Martin E, Lorenz S, Galler R. Tunnel boring machine performance prediction with scaled rock cutting tests. *International Journal of Rock Mechanics and Mining Sciences*, 2014, 70(9): 450–459
 25. Wu F, Yin L J, Zhang H, Gong Q M. Rock fragmentation mechanism and efficiency under inserted-tooth roller cutter by rotary cutting test. *China Journal of Highway and Transport*, 2018, 31(10): 150–159 (in Chinese)
 26. Geng Q, Wei Z Y, Meng H. An experimental research on the rock cutting process of the gage cutters for rock tunnel boring machine (TBM). *Tunnelling and Underground Space Technology*, 2016, 52: 182–191
 27. Geng Q, Wei Z Y, Meng H, Macias F J. Mechanical performance of TBM cutterhead in mixed rock ground conditions. *Tunnelling and Underground Space Technology*, 2016, 57: 76–84
 28. Geng Q, He F, Ma M X, Liu X H, Wang X B, Zhang Z Y, Ye M. Application of full-scale experimental cutterhead system to study penetration performance of tunnel boring machines (TBMs). *Rock Mechanics and Rock Engineering*, 2022, 55(8): 4673–4696
 29. Liu H Y, Kou S Q, Lindqvist P A, Tang C A. Numerical modelling of the heterogeneous rock fracture process using various test techniques. *Rock Mechanics and Rock Engineering*, 2007, 40(2): 107–144 (in Chinese)
 30. Su W L, Li X G, Xu Y, Jin D L. Numerical simulation of shield tool cutting concrete based on HJC model. *Journal of Zhejiang University (Engineering Science)*, 2020, 54(6): 1106–1114 (in Chinese)
 31. Tan Q, Yi N E, Xia Y M, Xu Z J, Zhu Y, Song J H. Research on rock dynamic fragmentation characteristics by TBM cutters and cutter spacing optimization. *Chinese Journal of Rock Mechanics and Engineering*, 2012, 31(12): 2453–2464 (in Chinese)
 32. Haeri H, Marji M F, Shahriar K. Simulating the effect of disc erosion in TBM disc cutters by a semi-infinite DDM. *Arabian Journal of Geosciences*, 2015, 8(6): 3915–3927
 33. Haeri H, Marji M F. Simulating the crack propagation and cracks coalescence underneath TBM disc cutters. *Arabian Journal of Geosciences*, 2016, 9(2): 124
 34. Ren D J, Shen J S, Chai J C, Zhou A. Analysis of disc cutter failure in shield tunnelling using 3D circular cutting theory. *Engineering Failure Analysis*, 2018, 90: 23–35
 35. Wen S, Wu F, Li S, Zhang L M. Numerical simulation of rock fragmentation efficiency of TBM disc cutter under different lateral pressure coefficient and rock strength. *Hazard Control in Tunnelling and Underground Engineering*, 2021, 3(4): 9–19
 36. Holmquist T J, Johnson G R. A computational constitutive model for glass subjected to large strains, high strain rates and high pressures. *Journal of Applied Mechanics*, 2011, 78(5): 051003
 37. Lewis B A. *Manual for LS-DYNA Soil Material Model 147 (No. FHWA-HRT-04-095)*. 2004
 38. Simo J C, Ju J W. Strain- and stress-based continuum damage models—I. Formulation. *International Journal of Solids and Structures*, 1987, 23(7): 821–840
 39. Simo J C, Ju J W. Strain- and stress-based continuum damage models—II. Computational aspects. *International Journal of Solids and Structures*, 1987, 23(7): 841–869
 40. Ju J W. On energy-based coupled elastoplastic damage theories: Constitutive modeling and computational aspects. *International Journal of Solids and Structures*, 1989, 25(7): 803–833
 41. Ju J W. Energy-based coupled elastoplastic damage models at finite strains. *Journal of Engineering Mechanics*, 1989, 115(11): 2507–2525
 42. Murray Y D. Modeling rate effects in rock and concrete. In: *Proceedings of the 8th International Symposium on the Interaction of the Effects of Munitions with Structures*. Washington, D.C., 1997, 65–79
 43. GB/T 50081-2002. *Standard for Test Method of Mechanical*

- Properties on Ordinary Concrete. Beijing: China Architecture & Building Press, 2002 (in Chinese)
44. JGJ 55-2011. Specification for Mix Proportion Design of Ordinary Concrete. Beijing: China Architecture & Building Press, 2011 (in Chinese)
45. JGJ/T 98-2010. Specification for Mix Proportion Design of Masonry Mortar. Beijing: China Architecture & Building Press, 2010 (in Chinese)
46. GB/T 50123-2019. Standard for Soil Test Method. Beijing: China Architecture & Building Press, 2019 (in Chinese)